Size distribution spectrum of noninertial particles in turbulence

Izumi Saito,* Toshiyuki Gotoh, and Takeshi Watanabe
Department of Physical Science and Engineering, Nagoya Institute of Technology, Nagoya 466-8555, Japan

(Received 25 January 2018; revised manuscript received 29 April 2018; published 24 May 2018)

Collision-coalescence growth of noninertial particles in three-dimensional homogeneous isotropic turbulence is studied. Smoluchowski's coagulation equation describes the evolution of the size distribution of particles in this system. By applying a methodology based on turbulence theory, the equation is shown to have a steady-state solution, which corresponds to the Kolmogorov-type power-law spectrum. Direct numerical simulations of turbulence and Lagrangian particles are conducted. The result shows that the size distribution in a statistically steady state agrees accurately with the theoretical prediction.

DOI: 10.1103/PhysRevE.97.053108

I. INTRODUCTION

Coagulation growth of particles plays an important role in various phenomena, such as growth of aerosol particles in the atmosphere [1,2], raindrop formation in an atmospheric cloud [2,3], planetesimal formation in protoplanetary disks [4,5], and sol-gel transformation in polymerizing systems [6].

When the number of particles is huge and it is difficult to track the motion of each particle, the evolution of the particle size distribution is often considered instead. Here, $n(\sigma,t)d\sigma$ is defined as the number of particles having a volume of between σ and $\sigma+d\sigma$ per unit volume of fluid media at time t. The evolution of the size distribution $n(\sigma,t)$ due to collision-coalescence is assumed to be described by the Smoluchowski equation [7] as

$$\begin{aligned}\frac{dn(\sigma,t)}{dt} = {} & \frac{1}{2}\int_0^\sigma\int_0^\sigma K(\sigma_1,\sigma_2)n_1n_2\delta(\sigma-\sigma_1-\sigma_2)d\sigma_1d\sigma_2 \\ & -\frac{1}{2}\int_0^\infty\int_0^\infty K(\sigma,\sigma_2)nn_2\delta(\sigma_1-\sigma-\sigma_2)d\sigma_1d\sigma_2 \\ & -\frac{1}{2}\int_0^\infty\int_0^\infty K(\sigma,\sigma_1)nn_1\delta(\sigma_2-\sigma-\sigma_1)d\sigma_1d\sigma_2 \\ & +I+S, \end{aligned} \tag{1}$$

where $n_i = n(\sigma_i,t)$ $(i=1,2)$, $\delta()$ is the Dirac δ function, and the collision kernel $K(\sigma_1,\sigma_2)$ indicates the rate at which a pair of particles with volumes σ_1 and σ_2 merge and form a particle of volume $\sigma=\sigma_1+\sigma_2$. The terms I and S represent a source and sink of particles, respectively.

Recently, a theory was proposed to derive a steady-state solution for (1) [8–10]. This theory uses similarities between the Smoluchowski equation (1) and the kinetic equation, the governing equation in wave turbulence theory which describes the evolution of the energy spectrum in wave-number space [10,11]. As usual in turbulence studies, a statistically steady state under the presence of a source (I) and sink (S) of particles is considered in (1). After injection by the source around the size σ_I, particles merge and grow in size, and finally they are removed by the sink around the size σ_S, where $\sigma_I \ll \sigma_S$. In a size range where the effects of both source and sink are assumed to be small ($\sigma_I \ll \sigma \ll \sigma_S$), a Kolmogorov-type power-law distribution [$n(\sigma) \sim \sigma^\nu$, where ν is a constant] is derived as a formal solution after the Zakharov transformation. The derivation assumes that mergings of particles with comparable sizes are dominant in the coagulation interaction associated with the solution. This property is called locality in the size interaction, which corresponds to locality in the scale interaction in turbulence theory [10–12]. Locality of the size interaction can be examined *a posteriori* by substituting the derived solution into (1) and checking the finiteness of the collision integral. When the integral is finite, the assumption of the interaction locality is confirmed and the solution is established in the range $\sigma_I \ll \sigma \ll \sigma_S$ in a statistically steady state.

Horvai *et al.* (2008) [9] (hereinafter referred to as HNS) applied this theory to spherical particles falling at their terminal velocities in a stationary fluid under the influence of uniform gravity and Stokes drag. HNS considered two simplified models for particle coalescence; either any particle pair coalesces when their trajectories cross (referred to as "free merging") or coalescence is restricted to similar-sized particles (referred to as "forced locality"). For the case of forced locality, HNS derived a power-law solution of the Smoluchowski equation in a steady state and showed that it is given by $n(\sigma) \propto \sigma^{-13/6}$. They also conducted direct numerical simulations (DNSs) by calculating the Lagrangian evolution of particles, and demonstrated that the size distribution close to the theoretical prediction is established in a statistically steady state.

In HNS, the trajectory of a particle is uniquely determined once it is introduced at a certain position in the system, because particles are assumed to move straight in the direction of the gravity force at their terminal velocities. The collision rate is determined primarily by the difference in terminal velocities of particles and corresponds to the gravitational collision kernel $K(\sigma_1,\sigma_2) = \pi(r_1+r_2)^2|V_1-V_2|$, where V_i and $r_i[=(3\sigma_i/4\pi)^{1/3}]$ are the terminal velocity and radius, respectively, of a particle with volume σ_i $(i=1,2)$. Such a model is a good approximation for the collision of raindrops as considered by HNS and is actually used in various types

*izumi@gfd-dennou.org

of cloud models [13,14]. In general, however, it is also the case that the randomness in the motion of fluid media plays an important role in the transport, and hence collision statistics, of particles. For example, the randomness in the motion of fluid media due to turbulence has important effects on the collision growth of cloud droplets [15–17], planetesimals [4,6,18], etc.

In the present study, we consider the case in which the randomness of a turbulent flow field affects the collision statistics of particles. As a simplest model, we consider the collision-coalescence growth of spherical particles without inertia advected by three-dimensional homogeneous isotropic turbulence. In this case, the effect of the randomness of the turbulent flow field on the collision of particles is represented in the well-known Saffman-Turner turbulent collision kernel [19]:

$$K(\sigma_1,\sigma_2) = (r_1 + r_2)^3 \left(\frac{8\pi\epsilon}{15\nu_a}\right)^{1/2}, \tag{2}$$

where ν_a is the kinematic viscosity of the fluid and ϵ is the energy dissipation rate. For coalescence of particles, we follow HNS and mainly consider the case with forced locality.

Another motivation of the present study is to examine the consistency between theory and DNS, thereby validating the accuracy of DNS, which uses a Lagrangian framework for particles and includes collision-coalescence. DNS is a useful tool and has been used in studies of the collision of particles [20,21]. Although many of them consider applications for situations that include not only collision but also coalescence, these studies often do not model coalescence explicitly and assume special forms of size distributions of particles, such as monodispersed and bidispersed distributions. It is recently that DNSs without such special assumptions have been conducted [17,22,23], and the accuracy of those DNSs have not yet sufficiently been validated with respect to the size distribution spectrum formed due to collision-coalescence of various sizes of particles. Our approach here examines the consistency of theory and DNS for a situation which includes explicit treatment of coalescence.

The remainder of the present paper is organized as follows. Section II presents the theory. The Kolmogorov-type power-law solution for the Smoluchowski equation (1) is derived. Locality of the size interaction associated with the derived solution is also examined, and an analytical form of the constant coefficient for the solution is derived. In Sec. III, we conduct DNSs and show that the theoretically predicted size distribution is reproduced accurately in a statistically steady state. A summary and discussion are provided in Sec. IV.

II. KOLMOGOROV-TYPE POWER-LAW SOLUTION

The procedure to derive a Kolmogorov-type power-law distribution as a steady-state solution is the same as that in HNS, except for the form of the collision kernel (2). Readers are referred to HNS for more details concerning the derivation and the theoretical background.

We consider a statistically steady state ($d/dt = 0$) in (1). Particles are injected into the system by the source around the size σ_I. They grow in size by merging, and are removed from the system by the sink around the size σ_S. We assume that $\sigma_I \ll \sigma_S$ and that the effects of both source and sink are small in the size range $\sigma_I \ll \sigma \ll \sigma_S$. In this range, the source and sink terms can be neglected. Equation (1) is rewritten in the same form as the kinetic equation in wave turbulence theory as follows:

$$0 = \int_0^\infty\int_0^\infty (R_{\sigma\sigma_1\sigma_2} - R_{\sigma_1\sigma\sigma_2} - R_{\sigma_2\sigma\sigma_1})d\sigma_1 d\sigma_2, \tag{3}$$

where $R_{\sigma\sigma_1\sigma_2}$ is defined as

$$R_{\sigma\sigma_1\sigma_2} = \frac{1}{2}\left(\frac{3\epsilon}{10\pi\nu_a}\right)^{1/2}\left(\sigma_1^{1/3} + \sigma_2^{1/3}\right)^3 \times n_1 n_2 \delta(\sigma - \sigma_1 - \sigma_2). \tag{4}$$

We assume a power-law solution $n(\sigma) \approx \sigma^\nu$ in (3). After substituting $(\sigma_1,\sigma_2) = (\sigma\sigma_1',\sigma\sigma_2')$ for $R_{\sigma\sigma_1\sigma_2}$, we obtain

$$R_{\sigma\sigma_1\sigma_2} = \frac{1}{2}\left(\frac{3\epsilon}{10\pi\nu_a}\right)^{1/2}\sigma^{2\nu}[(\sigma_1')^{1/3} + (\sigma_2')^{1/3}]^3 \times (\sigma_1')^\nu(\sigma_2')^\nu\delta(1-\sigma_1'-\sigma_2') = \sigma^{2\nu}R_{1\sigma_1'\sigma_2'}, \tag{5}$$

and the first integrand in (3) is written as

$$\int_0^\infty\int_0^\infty \sigma^{2\nu+2}R_{1\sigma_1'\sigma_2'}d\sigma_1'd\sigma_2'. \tag{6}$$

Next, we apply the *Zakharov transformation* ([10,11,24,25], see also [8,9,26]) to the second and third integrands in (3). The purpose of this transformation is to extract the same factor $\sigma^{2\nu+2}R_{1\sigma_1'\sigma_2'}$ as in (6). The transformation is to substitute

$$(\sigma_1,\sigma_2) = (\sigma/\sigma_1',\sigma\sigma_2'/\sigma_1') \tag{7}$$

and

$$(\sigma_1,\sigma_2) = (\sigma\sigma_1'/\sigma_2',\sigma/\sigma_2') \tag{8}$$

into the second and third integrands in (3), respectively. First, after the substitution (7), the second integrand in (3) can be written as

$$\int_0^\infty\int_0^\infty \sigma^{2\nu+2}(\sigma_1')^{-3-2\nu}R_{1\sigma_1'\sigma_2'}d\sigma_1'd\sigma_2'. \tag{9}$$

Second, after the substitution (8), the third integrand in (3) can be written as

$$\int_0^\infty\int_0^\infty \sigma^{2\nu+2}(\sigma_2')^{-3-2\nu}R_{1\sigma_1'\sigma_2'}d\sigma_1'd\sigma_2'. \tag{10}$$

In summary, Eq. (3) is transformed into the following form:

$$0 = \sigma^{2\nu+2}\int_0^\infty\int_0^\infty \left(1-\sigma_1^{-3-2\nu}-\sigma_2^{-3-2\nu}\right)R_{1\sigma_1\sigma_2}d\sigma_1 d\sigma_2, \tag{11}$$

after dropping the primes. Since $R_{1\sigma_1\sigma_2}$ includes the Dirac δ function $\delta(1-\sigma_1-\sigma_2)$, the right-hand side of the above equation is identically zero if $(1-\sigma_1^{-3-2\nu}-\sigma_2^{-3-2\nu}) = (1-\sigma_1-\sigma_2)$, or $\nu = -2$. Then,

$$n(\sigma) \approx \sigma^{-2} \tag{12}$$

is a steady-state solution.

A. Locality of the solution

The above derivation assumes that the effects of both source and sink are small. In other words, the size distribution in the range $\sigma_I \ll \sigma \ll \sigma_S$ is assumed to be independent of the

characteristic sizes for the source (σ_I) and sink (σ_S) at a steady state. This corresponds to the assumption of locality in the size interaction, meaning that coagulations of similar-sized particles are dominant. Here, we check the validity of this assumption for the solution (12).

We perform the same analysis as described in HNS (see Appendix A for details). We consider the Smoluchowski equation (1) before the Zakharov transformation, examine the asymptotic behavior of the collision integrals for small and large sizes, and check the finiteness of the integrals after substituting the solution (12) into them. It is shown that the coagulation interaction is local on small and large sizes of particles if the following integration,

$$\int n\sigma d\sigma, \tag{13}$$

is finite for $\sigma \to 0$ and $\sigma \to +\infty$, respectively. Substituting $n \approx \sigma^{-2}$ into (13), we obtain

$$\int \sigma^{-2}\sigma d\sigma = \ln\sigma + \text{const.} \tag{14}$$

Since the integration diverges for both $\sigma \to 0$ and $\sigma \to +\infty$, the interaction is nonlocal. The assumption of the interaction locality does not apply, and the distribution (12) is not established at a steady state.

B. Forced locality

Here, we introduce the collision efficiency to enforce locality on the size interaction of particles. The Smoluchowski equation (1) assumes that particles of any size collide. However, when the trajectories of nearby particles are affected by the flow field around them, the smaller particle tends to circumvent the larger particle by tracking the stream line around it, and the collision probability tends to be smaller for a particle pair with a larger size ratio. This phenomenon is called hydrodynamic interaction, and its effect can be introduced in Eq. (3) by using the collision efficiency $\mathcal{E}$ as

$$0 = \int_0^\infty\int_0^\infty \left(R_{\sigma\sigma_1\sigma_2}\mathcal{E}_{\sigma_1\sigma_2} - R_{\sigma_1\sigma\sigma_2}\mathcal{E}_{\sigma\sigma_2} - R_{\sigma_2\sigma\sigma_1}\mathcal{E}_{\sigma\sigma_1}\right)d\sigma_1 d\sigma_2. \tag{15}$$

Here, $\mathcal{E}_{\sigma_1\sigma_2}$ indicates the collision efficiency of a particle pair with volumes σ_1 and σ_2. Generally, $\mathcal{E}_{\sigma_1\sigma_2}$ is a complicated function of σ_1, σ_2 and other parameters [13]. In the present study, however, we adopt the same strategy as HNS and use the simplest form of $\mathcal{E}_{\sigma_1\sigma_2}$ to include the effect of hydrodynamic interaction:

$$\mathcal{E}_{\sigma_1\sigma_2} = \begin{cases} 1 & \text{if } 1/q < r_1/r_2 < q \\ 0 & \text{otherwise} \end{cases}, \tag{16}$$

where $r_1/r_2 = (\sigma_1/\sigma_2)^{1/3}$ is the radius ratio of the two particles and the constant parameter $q(>1)$ represents the cutoff for the size interaction. This means that collisions are restricted to particle pairs with a radius ratio of between $1/q$ and q.

The collision integral in (15) is finite with the collision efficiency given by (16). Hence, the size interaction in this case is local, and the Kolmogorov-type power-law distribution is established in the size range $\sigma_I \ll \sigma \ll \sigma_S$ at a steady state. Because all three coefficients $\mathcal{E}$ in (15) are transformed into $\mathcal{E}_{\sigma_1'\sigma_2'}$ by Zakharov transformation when $\mathcal{E}$ is defined as (16), we obtain the same equation as (11) except that $R_{1\sigma_1\sigma_2}$ is multiplied by $\mathcal{E}_{\sigma_1\sigma_2}$:

$$0 = \sigma^{2\nu+2}\int_0^\infty\int_0^\infty \left(1-\sigma_1^{-3-2\nu} - \sigma_2^{-3-2\nu}\right)\mathcal{E}_{\sigma_1\sigma_2}R_{1\sigma_1\sigma_2}d\sigma_1 d\sigma_2. \tag{17}$$

Therefore, the solution is the same as (12). As in HNS, we hereinafter refer to the coefficient (16) as forced locality.

C. Nondimensional constant

The advantage of the Zakharov transformation is that it can determine the constant coefficient for the solution (12) in addition to the slope ν. From arguments similar to those presented in [8], an analytical form of (12) with the constant coefficient is derived as follows:

$$n(\sigma) = K_0 J_0^{1/2}(\nu_a/\epsilon)^{1/4}\sigma^{-2}, \tag{18}$$

where J_0 is the particle volume injection rate from a source and K_0 is a nondimensional constant. The derivation of (18) is described in Appendix B. The nondimensional constant K_0, given in (B9), depends on forced locality and is written as

$$K_0 = 2\left(\frac{10\pi}{3}\right)^{1/4}\left[\left.\frac{dI(\nu)}{d\nu}\right|_{\nu=-2}\right]^{-1/2}, \tag{19}$$

where the integration $I(\nu)$ is given in (B4). After differentiating $I(\nu)$ with respect to ν and substituting $\nu = -2$, we have

$$\begin{aligned}\left.\frac{dI(\nu)}{d\nu}\right|_{\nu=-2} &= -\int_0^\infty\int_0^\infty \frac{(2\ln\sigma_1)\sigma_1 + (2\ln\sigma_2)\sigma_2}{\sigma_1^2\sigma_2^2}\left(\sigma_1^{1/3}+\sigma_2^{1/3}\right)^3 \\ &\quad\times \mathcal{E}_{\sigma_1\sigma_2}\delta(1-\sigma_1-\sigma_2)d\sigma_1 d\sigma_2.\end{aligned} \tag{20}$$

Using the form of forced locality (16) and integrating (20) with respect to σ_2, we have

$$\left.\frac{dI(\nu)}{d\nu}\right|_{\nu=-2} = \int_{\sigma_{\min}}^{\sigma_{\max}} \frac{(2\ln\sigma_1)\sigma_1 + [2\ln(1-\sigma_1)](1-\sigma_1)}{\sigma_1^2(1-\sigma_1)^2} \times\left[\sigma_1^{1/3} + (1-\sigma_1)^{1/3}\right]^3 d\sigma_1, \tag{21}$$

where

$$\sigma_{\min} = (1+q^3)^{-1}, \quad \sigma_{\max} = 1-(1+q^3)^{-1}. \tag{22}$$

For example, $(\sigma_{\min},\sigma_{\max}) = (0.49,0.51)$ for $q = 1.02$, and $(\sigma_{\min},\sigma_{\max}) = (0.01,0.99)$ for $q = 5$. We numerically calculate the integration (21).

Figure 1(a) shows the relationship between the nondimensional constant K_0 and the cutoff parameter q. K_0 is typically order 0.1 and a decreasing function of q. The dependence of K_0 on q is interpreted as follows: the greater q means the wider range of particle size involved in the size interaction, leading to enhancement of the particle volume transfer by the size interaction in σ space and to smaller K_0. In the

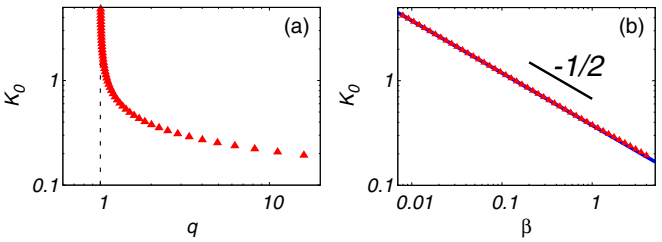

FIG. 1. (a) Nondimensional constant K_0 in (19) as a function of the cutoff parameter q for forced locality defined in (16). The data points are from $q = 1.004$ to $q = 16$. (b) Same as (a) except that the horizontal axis is $\beta = \log_2(q)$. The blue line ($\propto \beta^{-1/2}$) is the asymptotic form of K_0 for $\beta \approx 0$ given in (26). The short black line indicates a slope of $-1/2$.

case of $q = 2$,

$$K_0(q = 2) = 0.377\ldots \approx 0.38. \tag{23}$$

An asymptotic form of K_0 is obtained by setting

$$q = 2^{\beta} \tag{24}$$

and Taylor expanding (21) around $\beta = 0$. The expansion is given as

$$\left.\frac{dI(\nu)}{d\nu}\right|_{\nu=-2} = 192(\ln 2)^2\beta + \cdots, \tag{25}$$

hence we have

$$K_0 \approx \frac{1}{4\sqrt{3}(\ln 2)}\left(\frac{10\pi}{3}\right)^{1/4}\beta^{-1/2} = (0.3746\ldots)\times\beta^{-1/2}. \tag{26}$$

Figure 1(b) compares (26) with numerically calculated K_0. The agreement between the two is excellent, remarkably even for $\beta > 1$.

III. DIRECT NUMERICAL SIMULATIONS

In this section, we conduct DNSs of particles advected in three-dimensional homogeneous isotropic turbulence and compare the results with the theoretical prediction obtained in the previous section.

A. Experimental setup

The velocity field of a fluid is governed by the incompressible Navier-Stokes equations:

$$\frac{\partial \mathbf{u}}{\partial t} + \mathbf{u}\cdot\nabla\mathbf{u} = -\frac{1}{\rho_a}\nabla p + \nu_a\nabla^2\mathbf{u} + \mathbf{f}, \quad \nabla\cdot\mathbf{u} = 0, \tag{27}$$

where ρ_a is the density and $\mathbf{f}$ represents the external force. We set $\rho_a = 1.06\times10^{-3}$ g cm^{-3} and $\nu_a = 0.15$ cm^2 s^{-1}, which are typical values for the terrestrial atmosphere. Particles are regarded as spherical point masses without inertia that are advected by the fluid velocity at the particle position. The evolution equations for the position of the jth particle, $\mathbf{X}_j(t)$, are

$$\frac{d\mathbf{X}_j}{dt} = \mathbf{u}(\mathbf{X}_j), \tag{28}$$

where $\mathbf{u}(\mathbf{X}_j)$ is the fluid velocity at $\mathbf{X}_j$. $\mathbf{u}(\mathbf{X}_j)$ is calculated from the velocity field at the surrounding eight grid points by linear interpolation.

We use the same collision detection scheme as that used in [22]. The number density of particles is kept sufficiently small, so that only binary collisions are considered. Collisions of two particles are detected if their trajectories overlap. When particles coalesce, the total mass is conserved. More detailed explanations are provided in [22].

In the present simulation, we consider the case with forced locality (16) and set $q = 2$. This means that a particle pair with a radius ratio smaller than 2 coalesces if their trajectories overlap. The case without forced locality may also be interesting. However, this case requires more careful considerations of sources and sinks, because the size distribution is expected to be sensitive to precise forms of sources and sinks due to nonlocal size interactions. Thus, we leave this as a task for future study and herein consider the simplest case with forced locality (16).

The numerical domain is a cubic box with a length $L_{box} = 25.6$ cm per side. Periodic boundary conditions in three directions are imposed on the flow field. We numerically integrate the evolution equations (27) and (28) using the second-order Runge-Kutta scheme. For spatial discretization of the flow field, we use the pseudo spectral method with a grid number $N = 256$ for each direction and a grid spacing $\Delta x = L_{box}/N = 1$ mm. The force $\mathbf{f}$ is solenoidal, is applied to all wave-number components within a shell of $4 \leqslant kL_{box} \leqslant 6$, and is produced by an Ornstein-Uhlenbeck stochastic process, the details of which are explained in [22]. Turbulence parameters are summarized in the row "run 1" in Table I. Definitions of turbulence parameters are given in Appendix C.

TABLE I. Numerical and mean turbulence parameters. R_λ is the Taylor microscale Reynolds number, E is the kinetic energy, ϵ is the mean energy dissipation rate per unit mass, $\mathcal{L}$ is the integral scale, λ is the Taylor microscale, η is the Kolmogorov length, $k_{max}\eta$ is the cutoff wave number normalized by the Kolmogorov length, T_{eddy} is the large-eddy turnover time, and τ_K is the Kolmogorov time. Definitions of parameters are given in Appendix C.

	R_λ	E [cm^2 s^{-2}]	ϵ [cm^2 s^{-3}]	$\mathcal{L}$ [cm]	λ [cm]	η [mm]	$k_{max}\eta$	T_{eddy} [s]	τ_K [s]
Run 1	27.5	17.2	17.5	1.93	1.22	1.18	3.42	0.57	9.27×10^{-2}
Run 2	27.5	17.2	17.5	1.93	1.22	1.18	3.42	0.57	9.27×10^{-2}
Run 3	39.6	55.0	85.8	1.76	0.98	0.792	2.30	0.29	4.18×10^{-2}

TABLE II. Particle parameters. Q_0 is the particle number injection rate, J_0 is the injection rate of the volume of particles [see (29) for the definition], and $\overline{n}$ and N_p are the mean number density and total number of particles, respectively, in a statistically steady state.

	Q_0 [cm^{-3} s^{-1}]	J_0 [s^{-1}]	$\overline{n}$ [cm^{-3}]	N_p
Run 1	4.77×10^{-1}	3.49×10^{-8}	629	1.06×10^{7}
Run 2	2.98×10^{-2}	2.18×10^{-9}	157	2.64×10^{6}
Run 3	4.77×10^{-1}	3.49×10^{-8}	427	7.16×10^{6}

We first integrate the evolution equation for the flow field (27) without particles until a steady state is reached for turbulence statistics. Typically, this takes a few large-eddy turnover times. We then add particles into the system and integrate evolution equations both for the flow field (27) and particles (28). Turbulence is in a statistically steady state in all results shown and, unless explicitly stated otherwise, a phrase "statistically steady state" hereinafter refers to a steady state in terms of particle statistics.

Particles are injected into the system at a constant rate Q_0, namely, Q_0 new particles are introduced per unit volume of fluid per unit time. For run 1, $Q_0(\text{run 1}) = 0.477$ cm^{-3} s^{-1}. The initial positions of injected particles in the domain are random. Their initial radii are between 21.4 and 30.0 μm, determined by a uniform random number generator. As soon as the radius of a particle exceeds 1000 μm, the particle is removed from the system. The mean particle number density at a statistically steady state is approximately $\overline{n}(\text{run 1}) = 629$ cm^{-3}.

The relation between the particle number injection rate Q_0 and the particle volume injection rate J_0 is given by

$$J_0 = Q_0 \times \int_0^\infty P(r)\sigma(r)dr, \tag{29}$$

where $P(r)$ is the probability density function for the radius of injected particles. For the case of a uniform distribution, $P(r) = (r_2 - r_1)^{-1}$ for $r_1 \leqslant r \leqslant r_2$ and $P(r) = 0$ for otherwise, and we obtain

$$J_0 = Q_0\left(\frac{\pi}{3}\right)\left(r_2^2 + r_1^2\right)(r_2 + r_1). \tag{30}$$

Substituting $(r_1, r_2) = (21.4, 30.0) \times 10^{-4}$ cm and $Q_0(\text{run 1}) = 0.477$ cm^{-3} s^{-1}, we obtain $J_0(\text{run 1}) = 3.49 \times 10^{-8}$ s^{-1}.

In addition to run 1, we conduct two additional experiments in order to check the parameter dependence of the result. For run 2, the particle number injection rate is reduced to 1/16 of that of run 1, $Q_0(\text{run 2}) = 1/16 \times Q_0(\text{run 1})$. For run 3, the force amplitude is changed so that the mean energy injection rate is increased from $\epsilon(\text{run 1}) = 17.5$ cm^2 s^{-3} to $\epsilon(\text{run 3}) = 85.8$ cm^2 s^{-3}. The other turbulence and particle parameters are summarized in Tables I and II, respectively.

For numerical simulations, we use a cloud microphysics simulator, which is a DNS model for cloud turbulence and has been developed in previous studies [22,27]. The supercomputers used in the present study are the K-computer at the Research Organization for Information Science and Technology (RIST) in Kobe and the Fujitsu FX100 installed at Nagoya University. Parallelization of the computer program was developed and described in [22,27]. The time increment is chosen so that the CFL condition for the turbulence is satisfied, and $\Delta t = 10^{-3}$ s for all runs. As explained later in Fig. 4, reaching a statistically steady state takes a long time, over 8000 s (or eight million steps with $\Delta t = 10^{-3}$ s). These computations are conducted with 4096 cores and the corresponding CPU time is over 110 h.

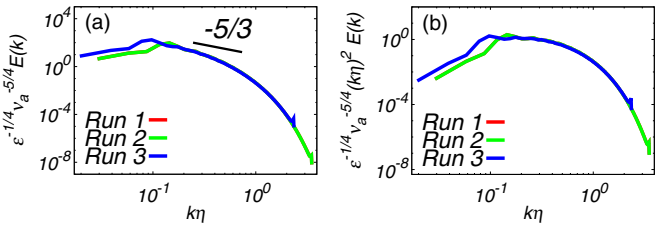

FIG. 2. (a) Time-averaged kinetic energy spectra normalized by Kolmogorov units: $\epsilon^{-1/4}\nu_a^{-5/4}E(k)$. (b) Time-averaged dissipation spectra normalized by Kolmogorov units: $\epsilon^{-1/4}\nu_a^{-5/4}(k\eta)^2E(k)$. The results for runs 1–3 are indicated by the red, green, and blue curves, respectively. Note that the red and green curves are almost identical. The line in the left-hand panel indicates a slope of $-5/3$.

B. Results

Figure 2(a) shows the kinetic energy spectra for all runs at steady states in terms of turbulence statistics. Curves are normalized by Kolmogorov units. The time average of the spectrum is calculated from the data every 10 s over 1000 s (at least over 1500 large-eddy turnover times, see Table I) after a statistically steady state is attained for turbulence statistics. The peak of each spectrum is included in the wave-number range in which the external force is applied. For higher wave numbers, the slope of the spectra is steeper than $-5/3$, followed by exponential decay near the cutoff wave number. An inertial subrange with a slope of $-5/3$ is not clearly established due to small Reynolds numbers R_λ. Figure 2(b) shows the normalized dissipation spectra. Each spectrum in Fig. 2(b) exhibits exponential decay at higher wave numbers, and values near the cutoff wave number are at least 10^3 times smaller than the peak value. All runs have $k_{\max}\eta$ greater than 2, as shown in Table I. These results indicate that turbulence is sufficiently resolved [28,29].

Figure 3(a) shows the time average of the size distribution $n(\sigma,t)$ for run 1 in a statistically steady state. Here, the time average is calculated from the data every 10 s over 5000 s (at least over 7500 large-eddy turnover times) after a statistically steady state is attained for particle statistics. The distribution accurately reproduces the predicted slope of -2 in the volume range of 10^{-6}–10^{-4} cm^3, where the effects of particle injection and removal are small. Theory suggests that the transfer flux of the particle volume in this range is approximately constant, resulting in the *coagulation subrange* [2,30,31], which is analogous to the turbulence inertial subrange. When the particle radius r is considered instead of the volume σ for the size distribution, the theoretical prediction for the slope is determined by the transformation formula: $n(\sigma)d\sigma \propto n(\sigma)r^2dr = n(r)dr$. Thus, we have $n(r) \approx n(\sigma)r^2 = \sigma^{-2}r^2 \propto r^{-4}$.

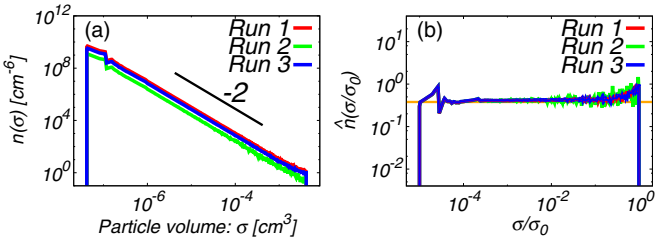

FIG. 3. (a) Time-averaged size distribution $n(\sigma)$ in a statistically steady state. The results for runs 1–3 are indicated by the red, green, and blue curves, respectively. The line indicates a slope of -2 from the theoretical prediction. (b) Same as (a), but the distributions are normalized by (34). The horizontal line indicates the nondimensional constant $K_0 = 0.38$ from the theoretical prediction (23).

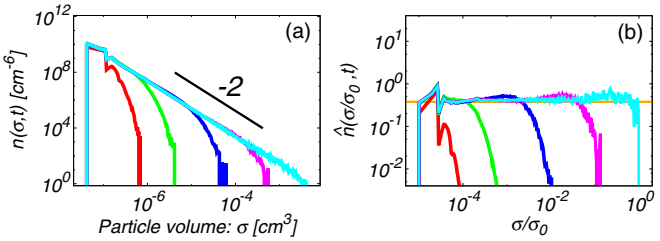

FIG. 4. (a) Snapshots of the size distribution $n(\sigma,t)$ for run 1 at $t = 500$ s (red), 2000 s (green), 4000 s (blue), 6000 s (purple), and 8000 s (cyan) from left to right. The short line indicates a slope of -2 from the theoretical prediction. (b) Same as (a), except that the distributions are normalized by (34). The horizontal line indicates the nondimensional constant $K_0 = 0.38$ from the theoretical prediction (23).

The nondimensional constant K_0 in (18) can be estimated from Fig. 3(a). We use the data for run 1 in the range $5 \times 10^{-6} < \sigma < 5 \times 10^{-5}$. Substituting the parameters and experimental results into (18), the mean value and standard deviation are

$$K_0^{\mathrm{DNS}} = 0.410 \pm 0.005, \tag{31}$$

for the case $q = 2$ in (16) considered in the present DNS. Since the theoretical prediction for $q = 2$ is $K_0 = 0.38$ as given in (23), the agreement between the theory and DNS is within 7%, which is fairly good. However, in view of the standard deviation of K_0^{DNS}, the DNS result slightly overestimates the value of the nondimensional constant.

There are two possible causes for the above overestimation. The first is that the overestimation comes from the overprediction in the Saffman-Turner kernel (2). Wang *et al.* [21] considered the monodispersed size distribution and demonstrated that the form (2) for the monodispersed case,

$$\Gamma_1 = (2r)^3 \left(\frac{8\pi\epsilon}{15\nu_{\mathrm{a}}} \right)^{1/2}, \tag{32}$$

tends to overpredict the kernel in comparison to the more accurate form,

$$\Gamma_2 = 2\pi\,(2r)^2 \overline{|w|}, \tag{33}$$

due to the assumptions in (32), where r is the particle radius and $\overline{|w|}$ is the mean relative velocity in the longitudinal direction between two points with a distance $2r$. For example, in their experiments with $R_\lambda = 24$, $\eta/\Delta x = 0.45$, and $r/\Delta x = 0.4$, they showed that the overprediction is about 4.9%, where 0.8% is from the assumption $R \ll \eta$ and 4.1% is from the Gaussian assumption of statistics for the turbulent flow field. In the present study, $R_\lambda = 27.5$, $\eta/\Delta x = 1.18$, and $0.02 \leqslant r/\Delta x \leqslant 1$. Thus, it is possible that Eq. (2) overpredicts the collision rate by a few percent. The second possibility is that the collision rate is underestimated in our DNS due to the linear interpolation scheme used for calculating the flow velocity at the particle position. Yokojima *et al.* [32] compared the linear and cubic interpolation schemes and demonstrated that DNSs with the linear interpolation scheme tends to underestimate the collision rate as compared to those with the cubic interpolation scheme. For example, in their experiments where $R_\lambda = 31.0$, $\eta/\Delta x = 1.19$, and $r/\Delta x = 0.60$, they showed that the underestimation is about 1.8%. Since the present DNS uses the linear interpolation scheme, it is possible that the collision rate is slightly underestimated. Both of the two possibilities discussed above are consistent with the overestimation of the nondimensional constant K_0 in our DNS (31) in comparison with the prediction (23).

According to the theoretical prediction (18), the size distribution $n(\sigma)$ can be normalized as

$$n(\sigma) = J_0^{1/2} (\nu_{\mathrm{a}}/\epsilon)^{1/4} \sigma^{-2} \hat{n}(\sigma/\sigma_0), \tag{34}$$

where $\hat{n}(\sigma/\sigma_0)$ is a nondimensional function, and σ_0 is the volume at which particles are removed. In the present simulation, σ_0 is the volume of the sphere with a radius of $r = 1000$ μm and $\sigma_0 = 4.19 \times 10^{-3}$ cm^3. Figure 3(b) shows the normalized size distribution $\hat{n}(\sigma/\sigma_0)$. In this figure, the horizontal line corresponds to the theoretical prediction and the nondimensional constant K_0.

The slope of the size distribution for $\sigma > 10^{-3}$ cm^3 in Fig. 3(a) is slightly shallower than -2, forming a small cusp in the right tail of the distribution. The cusp is more clearly seen in the normalized size distribution in Fig. 3(b). This cusp is formed due to the effect of particle removal. Since particles with radii greater than 1000 μm are removed in the present simulation, coagulation growth of particles for $\sigma > 10^{-3}$ cm^3 in Fig. 3(a) through interaction with removed particles is suppressed. In order to compensate for this suppression, the amplitude near the right tail becomes greater than the theoretical prediction, resulting in the shallower slope and the small cusp.

The results for different parameters (such as J_0, ϵ) are expected to collapse onto a single curve after the normalization described in (34). In order to confirm this, we conduct two additional experiments, runs 2 and 3. In run 2, the particle number injection rate Q_0 (and hence the volume injection rate J_0) is decreased to 1/16 of that of run 1. On the other hand, in run 3, the force amplitude is increased so that the mean energy injection rate is $\epsilon = 85.8$ cm^2 s^{-3}. The turbulence and particle parameters for runs 2 and 3 are summarized in Tables I and II, respectively. The normalized size distributions for runs 2 and 3 are plotted in Fig. 3(b) along with that for run 1, which exhibits almost perfect collapse.

Figure 4(a) shows snapshots of the evolution of the size distribution $n(\sigma,t)$ for run 1. As shown in the figure, attaining

a statistically steady state takes a long time, over 8000 s (or 13 000 large-eddy turnover time). The similarity between the evolution of the size distribution shown in Fig. 4(a) and the typical evolution of a power spectrum in turbulence theory (for example, see Fig. 3 in [33]) is striking. The distribution in Fig. 4(a) gradually broadens with time, extending the coagulation subrange (the range of -2 slope of the spectrum) as predicted from turbulence theory, and showing an approximately exponentially decaying right tail.

Let us estimate the timescale of the coagulation interaction by a simple scaling argument. We consider the Smoluchowski equation (1) with the Saffman-Turner kernel (2) without a source and sink, and substitute into it the characteristic scales for time (T_c) and particle volume (σ_c). Omitting constants, we have

$$\frac{n_c}{T_c} \approx \sigma_c \left(\frac{\epsilon}{\nu_a}\right)^{1/2} n_c n_c \sigma_c^{-1} \sigma_c \sigma_c, \tag{35}$$

where n_c is the characteristic magnitude for the size distribution with volume σ_c. Since n_c is estimated as

$$n_c \approx K_0 J_0^{1/2} \left(\frac{\epsilon}{\nu_a}\right)^{-1/4} \sigma_c^{-2} \tag{36}$$

from (18), we obtain

$$T_c \approx K_0^{-1} J_0^{-1/2} \left(\frac{\nu_a}{\epsilon}\right)^{1/4} = K_0^{-1} J_0^{-1/2} \tau_K^{1/2}, \tag{37}$$

where τ_K is the Kolmogorov time for fluid turbulence. Substituting $K_0 = 0.38$, J_0 and τ_K for run 1 (Tables I and II), we have $T_c \approx 4000$ s, which is roughly consistent with the time period ($\sim$8000 s) taken for attaining a statistically steady state in run 1.

We note two points about the coagulation timescale (37). First, the timescale is determined by three components: (1) the particle volume injection rate, (2) the Kolmogorov time, and (3) forced locality. The interpretation is as follows. The greater particle volume injection rate J_0 results in the greater particle number density, hence the higher collision rate and shorter timescale T_c. The shorter Kolmogorov time τ_K means the greater velocity gradient of fluid turbulence [19], hence the higher collision probability of particles and the shorter coagulation timescale T_c. The effect of forced locality is included in K_0. Second, the coagulation timescale (37) does not depend on the characteristic scale of particle volume σ_c. This is supported by Fig. 4(a), where the size distribution expands toward greater σ approximately 1 order of magnitude every 2000 s from $t = 2000$ s to 8000 s. Interestingly, such a relationship between the characteristic time and length scales is similar to that in two-dimensional turbulence, where the characteristic timescale for a given size of eddy in the enstrophy inertial subrange is independent of the eddy size apart from the logarithmic correction [34,35]. [This similarity suggests that the divergence of the collision integral discussed in (14) could be controlled by a logarithmic correction as in two-dimensional turbulence. But we do not delve into this problem further in the present study.]

Figure 4(b) shows the evolution of the nondimensional size distribution $\hat{n}(\sigma/\sigma_0, t)$ which has been normalized in the same manner as in (34). In each snapshot for $t \geqslant 4000$ s, the amplitude near the right tail is slightly greater than that in the middle part, forming a small bump near the right end of the distribution. Presumably, this bump is formed through a mechanism similar to that which causes the cusp in Fig. 3, which might correspond to the *bottleneck effect*, as observed in DNSs and large-eddy simulations (LESs) of turbulence [36–39].

IV. SUMMARY AND DISCUSSION

As the simplest model for the coagulation growth of particles in a turbulent flow, we investigated the collision-coalescence growth of noninertial particles advected in three-dimensional homogeneous isotropic turbulence. In this case, the probability of collision of a particle pair is given by the Saffman-Turner collision kernel (2). We considered a statistically steady state where particles are injected into the system by a source around the size σ_I, grow in size by merging, and are removed by a sink around the size σ_S. We considered the size range $\sigma_I \ll \sigma \ll \sigma_S$, where the effects of source and sink are assumed to be small. We applied a methodology developed in previous studies [8–10], which is based on turbulence theory, and derived a Kolmogorov-type power-law distribution $n(\sigma) \approx \sigma^{-2}$ as a formal solution of the Smoluchowski equation with the Saffman-Turner kernel. We also showed that the coagulation interaction associated with the derived solution is nonlocal and that the solution is not established without forced locality, a simplified model for hydrodynamic interaction that restricts the coagulation interaction to similar-sized particles. We then derived the analytical expression for the power-law distribution including the nondimensional constant K_0. We conducted direct numerical simulations (DNSs) of noninertial particles advected in three-dimensional homogeneous isotropic turbulence. The predicted slope of -2 was confirmed to be reproduced accurately in a statistically steady state. In addition, fairly good agreement between the theory and DNS was confirmed for the nondimensional constant K_0.

Although the present study is similar to the previous study by HNS [9], the following aspects of our work should be noted. The first is the accuracy of the steady-state size distribution reproduced by our DNS. The distribution reproduced by DNS in HNS (their Fig. 3) has sawtoothlike noise throughout the entire size range, and, based on their results, it was unclear whether this noise was of numerical origin. On the other hand, as shown in Fig. 3, the steady-state size distribution in our DNS accurately reproduced the theoretical prediction of the slope -2 in the middle part of the spectrum, where the effects of the source and sink are small. Such accurate results further made it possible to estimate the nondimensional constant K_0, which was demonstrated to agree fairly well with the theoretical prediction. The second is the difference in the mechanism which affects the collision statistics of particles. In contrast to the system considered in HNS where the collision statistics are mainly determined by differences in terminal fall velocities of particles, we considered the system where the collision statistics are affected by the randomness in the motion of fluid media due to turbulence. Collision-coalescence of particles in turbulence is relevant to various phenomena. Even though the present study uses many simplifying assumptions, such as ignoring particle inertia, the good agreement between theory and DNS shown in our results provides further support for the wider applicability

of turbulence theory to coagulation growth of particles in those phenomena, and encourages further studies in this direction.

We also found notable similarities between the size distribution of particles formed through collision growth in the present study and the energy spectrum associated with nonlinear interactions in turbulence. A bump was observed in the developing edge of the size distribution during its time evolution (Fig. 4). After a statistically steady state was attained, this bump was replaced by a small cusp in the right end of the distribution, where the sink effect occurs (Fig. 3). These bumps and cusps are reminiscent of the bottleneck effect observed in DNSs and LESs of fluid turbulence [36,37,39]. This is reasonable because the bottleneck effect is also predicted theoretically and confirmed by numerical simulations in wave turbulence, as described in Sec. 3.4.2 of [11]. As far as we know, however, the present study is the first to demonstrate the bottleneck effect in DNSs of collision-coalescence growth of particles.

The present study also provides validation for the accuracy of DNS, which uses a Lagrangian framework for particles and includes collision-coalescence [17,22,23]. The consistency between theory and DNS is confirmed with respect to the size distribution spectrum which is formed by the coagulation of various sizes of particles and derived as a formal solution of the Smoluchowski equation.

ACKNOWLEDGMENTS

I.S. is grateful to Dr. Taketo Ariki, Dr. Hideaki Mouri, and Prof. Keiichi Ishioka for fruitful discussions and instructive comments. We also would like to thank two anonymous reviewers for helpful comments. This research used the computational resources of the K computer provided by the RIKEN Advanced Institute for Computational Science, through the High Performance Computing Infrastructure (HPCI) System Research Project (hp160085, hp170189). This research used the computational resources of the Earth Simulator supercomputer system operated by the Japan Agency for Marine-Earth Science and Technology. The computational support provided by Japan High Performance Computing and Networking, Large-scale Data Analyzing and Information Systems (JHPCN) (jh160012, jh170013) and High Performance Computing (HPC 2016) at Nagoya University is also gratefully acknowledged. This work was supported by MEXT KAKENHI through Grant No. 15H02218 and JSPS KAKENHI Grants No. 26420106, No. 18K03925, and No. 18K13611. This work was supported by the Research Institute for Mathematical Sciences, a Joint Usage/Research Center located in Kyoto University.

APPENDIX A: LOCALITY OF THE SOLUTION

Here, we check locality of the size interaction associated with the solution (12) based on the kernel (2) by performing the same analysis as described in Appendix 1 of HNS [9] (see also Sec. 3.1.2 in [11]). We define $f(\sigma_1,\sigma_2) = K(\sigma_1,\sigma_2)n_1n_2$. The collision integrals in the Smoluchowski equation (1) can be rewritten as

$$\int_{\sigma_{\min}}^{\sigma/2} f(\sigma_1,\sigma-\sigma_1)d\sigma_1 - \int_{\sigma_{\min}}^{\sigma_{\max}} f(\sigma_1,\sigma)d\sigma_1, \tag{A1}$$

where zero and infinity in the integration range are replaced by $\sigma_{\min}$ and $\sigma_{\max}$, respectively. We can further rearrange above integrals to separate terms with $\sigma_{\min}$ from those with $\sigma_{\max}$ as

$$\int_{\sigma_{\min}}^{\sigma/2} [f(\sigma_1,\sigma-\sigma_1) - f(\sigma_1,\sigma)]d\sigma_1 - \int_{\sigma/2}^{\sigma_{\max}} f(\sigma_1,\sigma)d\sigma_1. \tag{A2}$$

If the first and second integrals in (A2) are finite for $\sigma_{\min} \to 0$ and $\sigma_{\max} \to \infty$, respectively, the coagulation interaction is local on small and large sizes of particles.

We first consider the case $\sigma_{\min} \to 0$. We should check the contribution from the integrand for small σ_1, or $\sigma_1 \ll \sigma$. The integrand in the first integral in (A2) is Taylor-expanded as

$$f(\sigma_1,\sigma-\sigma_1) - f(\sigma_1,\sigma) \approx \sigma_1\partial_\sigma[f(\sigma_1,\sigma)]. \tag{A3}$$

For $\sigma_1 \ll \sigma$, we get $f(\sigma_1,\sigma) \approx \sigma n_1 n$ from (2), and the first integral in (A2) is approximately written as

$$\left[\int_{\sigma_{\min}}^{\sigma/2} n_1\sigma_1 d\sigma_1\right]\partial_\sigma(\sigma n). \tag{A4}$$

We next consider the case $\sigma_{\max} \to \infty$. We should check the contribution from the integrand for large σ_1. For $\sigma_1 \gg \sigma$, we get $f(\sigma_1,\sigma) \approx \sigma_1 n_1 n$, and the second integral in (A2) is approximately written as

$$-n\left[\int_{\sigma/2}^{\sigma_{\max}} n_1\sigma_1 d\sigma_1\right]. \tag{A5}$$

Note that we obtain the same integrand as that in (A4).

From (A4) and (A5), the coagulation interaction is local on small and large sizes of particles if the following integration,

$$\int n_1\sigma_1 d\sigma_1, \tag{A6}$$

is finite for $\sigma_1 \to 0$ and $\sigma_1 \to \infty$, respectively.

APPENDIX B: ANALYTICAL FORM OF THE CONSTANT COEFFICIENT

Here, we derive an analytical form of the constant coefficient for the steady-state solution (12) with the collision coefficient (16). We express the size distribution as

$$n(\sigma) = C\sigma^{\nu}, \tag{B1}$$

and derive the form of a constant C for the case $\nu = -2$. The procedure is similar to that described in [8].

The continuity equation for the particle volume in σ space is expressed as

$$\frac{\partial}{\partial t}[\sigma n(\sigma,t)] = -\frac{\partial}{\partial\sigma}J(\sigma,t), \tag{B2}$$

where $J(\sigma,t)$ is the flux of the particle volume. Substituting the form (B1) into the Smoluchowski equation after the Zakharov transformation and comparing the result with (B2), we have

$$\frac{\partial}{\partial\sigma}J(\sigma,t) = C^2\sigma^{2\nu+3}\lambda I(\nu), \tag{B3}$$

where $\lambda = 2^{-1}(3\epsilon/10\pi\nu_a)^{1/2}$, and $I(\nu)$ is defined as

$$I(\nu) = -\int_0^\infty\int_0^\infty \left(1-\sigma_1^{-3-2\nu}-\sigma_2^{-3-2\nu}\right)\mathcal{E}_{\sigma_1\sigma_2}S_{1\sigma_1\sigma_2}d\sigma_1 d\sigma_2, \tag{B4}$$

where

$$S_{1\sigma_1\sigma_2} = \lambda^{-1} R_{1\sigma_1\sigma_2} = \left(\sigma_1^{1/3} + \sigma_2^{1/3}\right)^3 \sigma_1^{\nu}\sigma_2^{\nu}\,\delta(1-\sigma_1-\sigma_2). \quad \text{(B5)}$$

By integrating (B3), we have

$$J(\sigma,t) = C^2\lambda\sigma^{2\nu+4} \times \left(\frac{I(\nu)}{2\nu+4}\right). \quad \text{(B6)}$$

We consider a steady state with $\nu = -2$. From (B2) at a steady state, the flux J is constant and equal to J_0, the injection rate of particle volume from the source. Since both the numerator and denominator in the parenthesis in (B6) are zero for $\nu = -2$, we apply L'Hôpital's rule and obtain

$$J_0 = \frac{C^2\lambda}{2} \times \left.\frac{dI(\nu)}{d\nu}\right|_{\nu=-2}. \quad \text{(B7)}$$

Solving the above equation in terms of C and substituting $\lambda = 2^{-1}(3\epsilon/10\pi\nu_a)^{1/2}$, we have

$$C = K_0 J_0^{1/2} (\nu_a/\epsilon)^{1/4}, \quad \text{(B8)}$$

where

$$K_0 = 2\left(\frac{10\pi}{3}\right)^{1/4}\left[\left.\frac{dI(\nu)}{d\nu}\right|_{\nu=-2}\right]^{-1/2} \quad \text{(B9)}$$

is the nondimensional constant. Therefore, the steady-state solution is

$$n(\sigma) = K_0 J_0^{1/2} (\nu_a/\epsilon)^{1/4} \sigma^{-2}. \quad \text{(B10)}$$

APPENDIX C: DEFINITIONS OF TURBULENCE PARAMETERS

The kinetic energy is defined by

$$E = \frac{1}{2}\langle u_i^2\rangle = \int_0^\infty E(k)dk, \quad \text{(C1)}$$

where u_i $(i = 1,2,3)$ are components of velocity vector $\mathbf{u}$ (repeated indices are summed), the angle brackets $\langle\cdots\rangle$ represent the spatial and temporal averages, and $E(k)$ is the kinetic energy spectrum. The mean energy dissipation rate is defined by

$$\epsilon = \frac{\nu_a}{2}\langle(\partial_i u_j + \partial_j u_i)^2\rangle. \quad \text{(C2)}$$

The integral scale, Taylor microscale, and Kolmogorov scale are respectively defined by

$$\mathcal{L} = \left(\frac{3\pi}{4E}\right)\int_0^\infty k^{-1}E(k)dk, \quad \text{(C3)}$$

$$\lambda = \sqrt{\langle u_1^2\rangle/\langle(\partial_1 u_1)^2\rangle}, \quad \text{(C4)}$$

$$\eta = \left(\nu_a^3/\epsilon\right)^{1/4}. \quad \text{(C5)}$$

The large-eddy turnover time and Kolmogorov time are respectively defined by

$$T_{\text{eddy}} = \mathcal{L}/u_{\text{rms}}, \quad \text{(C6)}$$

$$\tau_K = (\nu_a/\epsilon)^{1/2}, \quad \text{(C7)}$$

where $u_{\text{rms}} = \sqrt{2E/3}$ is the root-mean-square velocity. The Taylor microscale Reynolds number is defined by

$$R_\lambda = u_{\text{rms}}\lambda/\nu_a. \quad \text{(C8)}$$

[1] S. H. Suck and J. R. Brock, J. Aerosol Sci. **10**, 581 (1979).
[2] H. R. Pruppacher and J. D. Klett, *Microphysics of Clouds and Precipitation* (Kluwer Academic Publishers, Dordrecht, 2011), p. 954.
[3] P. K. Wang, *Physics and Dynamics of Clouds and Precipitation* (Cambridge University Press, Cambridge, UK, 2013), p. 452.
[4] F. Brauer, C. P. Dullemond, and T. Henning, Astron. Astrophys. **480**, 859 (2008).
[5] S. Okuzumi, H. Tanaka, H. Kobayashi, and K. Wada, Astrophys. J. **752**, 106 (2012).
[6] E. Hendriks, M. Ernst, and R. Ziff, J. Stat. Phys. **31**, 519 (1983).
[7] M. V. Smoluchowski, Z. Phys. Chem. **92**, 215 (1917).
[8] C. Connaughton, R. Rajesh, and O. Zaboronski, Phys. Rev. E **69**, 061114 (2004).
[9] P. Horvai, S. V. Nazarenko, and T. H. M. Stein, J. Stat. Phys. **130**, 1177 (2008).
[10] S. V. Nazarenko, *Wave Turbulence*, Lecture Notes in Physics Vol. 825 (Springer, Berlin, 2011), p. 279.
[11] V. Zakharov, V. S. L'vov, and G. Falkovich, *Kolmogorov Spectra of Turbulence 1: Wave Turbulence* (Springer-Verlag, Berlin, 1992), p. 265.
[12] K. R. Sreenivasan and G. Stolovitzky, J. Stat. Phys. **78**, 311 (1995).
[13] W. D. Hall, J. Atmos. Sci. **37**, 2486 (1980).
[14] S. I. Shima, K. Kusano, A. Kawano, T. Sugiyama, and S. Kawahara, Q. J. R. Meteorol. Soc. **135**, 1307 (2009).
[15] O. Ayala, B. Rosa, L.-P. Wang, and W. W. Grabowski, New J. Phys. **10**, 075015 (2008).
[16] B. J. Devenish, P. Bartello, J.-L. Brenguier, L. R. Collins, W. W. Grabowski, R. H. A. IJzermans, S. P. Malinowski, M. W. Reeks, J. C. Vassilicos, L.-P. Wang, and Z. Warhaft, Q. J. R. Meteorol. Soc. **138**, 1401 (2012).
[17] R. Onishi, K. Matsuda, and K. Takahashi, J. Atmos. Sci. **72**, 2591 (2015).
[18] T. Ishihara, N. Kobayashi, K. Enohata, M. Umemura, and K. Shiraishi, Astrophys. J. **854**, 81 (2018).
[19] P. G. Saffman and J. S. Turner, J. Fluid Mech. **1**, 16 (1956).
[20] S. Sundaram and L. R. Collins, J. Fluid Mech. **335**, 75 (1997).
[21] L.-P. Wang, A. S. Wexler, and Y. Zhou, Phys. Fluids **10**, 266 (1998).
[22] I. Saito and T. Gotoh, New J. Phys. **20**, 023001 (2018).

[23] S. Chen, M. K. Yau, and P. Bartello, J. Atmos. Sci. **75**, 203 (2018).
[24] V. Zakharov and N. Filonenko, Dokl. Akad. Nauk SSSR **170**, 1292 (1966).
[25] V. Zakharov and N. Filonenko, Prikl. Mekh. Tekh. Fiz. **6**, 62 (1967).
[26] R. H. Kraichnan, Phys. Fluids **9**, 1728 (1966).
[27] T. Gotoh, T. Suehiro, and I. Saito, New J. Phys. **18**, 043042 (2016).
[28] V. Eswaran and S. B. Pope, Comput. Fluids **16**, 257 (1988).
[29] Y. Yamazaki, T. Ishihara, and Y. Kaneda, J. Phys. Soc. Jpn. **71**, 777 (2002).
[30] S. K. Friedlander, J. Meteorol. **17**, 373 (1960).
[31] S. K. Friedlander, J. Meteorol. **17**, 479 (1960).
[32] S. Yokojima, T. Mashiko, T. Matsuzaka, and T. Miyahara, Res. Inst. Math. Sci. Kokyuroku **1822**, 76 (2013).
[33] C. Connaughton, Physica D **238**, 2282 (2009).
[34] R. H. Kraichnan and D. Montgomery, Rep. Prog. Phys. **43**, 547 (1980).
[35] M. Lesieur, *Turbulence in Fluids* (Springer, The Netherlands, 2008), p. 558.
[36] W. Dobler, Nils Erland L. Haugen, T. A. Yousef, and A. Brandenburg, Phys. Rev. E **68**, 026304 (2003).
[37] D. A. Donzis and K. R. Sreenivasan, J. Fluid Mech. **657**, 171 (2010).
[38] G. Falkovich, Phys. Fluids **6**, 1411 (1994).
[39] P. Sagaut and V. Levasseur, Phys. Fluids **17**, 035113 (2005).